Nuclear Engineering and Technology 53 (2021) 2918–2925

Contents lists available at ScienceDirect

Nuclear Engineering and Technology

journal homepage: www.elsevier.com/locate/net

Original Article

Decontamination of spent ion exchange resins contaminated with iron-oxide deposits using mineral acid solutions

E.A. Tokar, A.I. Matskevich, M.S. Palamarchuk, Yu.A. Parotkina, A.M. Egorin*

Institute of Chemistry FEBRAS, 159 Pr-t 100-letiya Vladivostoka, Vladivostok, 690022, Russia

ARTICLE INFO

Article history:
Received 12 November 2020
Received in revised form
21 February 2021
Accepted 22 March 2021
Available online 29 March 2021

Keywords:
Ion exchange resins
Radioactive waste
Radionuclides
Decontamination

ABSTRACT

The efficiency of decontamination of model spent ion exchange resins, contaminated with magnetite and hematite, with mineral acid solutions, and using electro-decontamination, was evaluated. It has been shown that effective hematite dissolution occurs in concentrated mineral acid solutions. However, the use of direct current increases the decontamination efficiency of spent ion exchange resins contaminated with hematite. It is determined that with increasing voltage and acid concentration, the dissolution efficiency of hematite deposits increases and can exceed 99%. It has been shown that hematite dissolution is accompanied by secondary adsorption of radionuclides due to ion exchange, which can be removed with sodium nitrate solutions.

1. Introduction

The formation of iron oxide/hydroxide particles in the condensation water of the NPP circuit occurs due to the corrosion of steel elements; this process is enhanced by the radiolysis of water to form O_2 and H_2O_2 [1]. The dissolution of steel elements includes hydrolysis of the Fe^{3+} ion, the formation of amorphous oxo- and hydroxo-compounds, followed by their aging with the formation of the crystalline phases of hematite, goethite, and lepidocrocite [1,2]. Such particles have a common name – crud; their chemical composition is mainly represented by iron and to a lesser extent by chromium, nickel, cobalt, nickel, and zinc [3,4].

The crud presented in the circuit water accumulates radionuclides of the corrosive group, which leads to increased radiation burden of operational personnel [3]. Mechanical filtration on ion-exchange resins with subsequent backwashing is used to remove crud. As the number of filtered crud increases, the ion exchange capacity of resins decreases [5], which affects their performance negatively [2]. As the operating time of ion-exchange resins increases, the efficiency of mechanical removal of iron-oxide particles from the circuit water increases due to the "aging" effect, which manifests itself as a gradual decrease in the cross-linking degree of ion-exchangers, as well as an increase in the specific surface area of the resin grain [6,7]. The negative effect of "aging" is irreversible contamination of ion-exchangers due to the facilitated diffusion of crud particles into the pores of ion-exchangers during their aging [6], as well as the adsorption of Fe^{2+} and Fe^{3+} on the functional groups of the resin, with the formation of particles of oxo- and hydroxo-compounds in the volume of the resin grain directly [2]. Such particles can no longer be removed by backwashing, and the efficiency of their removal using chemical regeneration does not exceed 50% [6]. In this regard, the problem of processing spent ion-exchange resins contaminated with iron oxide particles becomes relevant. The residual activity of such spent ion exchange resin (SIER) during long-term storage will be determined by the gamma activity of Co-60 primarily [8], due to its longest half-life among short-lived radionuclides of the corrosive group.

Well-known methods of disposal of SIER, such as cementation, pyrolysis, and combustion, have some disadvantages, such as an increase in the final volume of radioactive waste [9], as well as the formation of secondary gaseous products, including radioactive ones [10,11]. Liquid-phase oxidation of SIER using the Fenton and electro-Fenton process allows the destruction of the polymer matrix of ion-exchangers at relatively low temperatures to form non-toxic products [12,13]. The significant consumption of concentrated hydrogen peroxide solution, as well as incomplete dissolution of the SIER matrix, still limits the use of these methods.

The use of chemical methods that do not lead to the destruction of the ion-exchanger polymer matrix is the most optimal method of processing since it allows reducing the volume of radioactive waste

* Corresponding author.
E-mail address: andrey.egorin@gmail.com (A.M. Egorin).

https://doi.org/10.1016/j.net.2021.03.022

by re-using decontaminating solutions. Decontaminated SIERs can later be buried in an urban waste landfill [14]. For example, this approach was successfully applied by the authors of this article to develop a scheme for the decontamination of SIER contaminated with silicate deposits [15].

The efficiency of removing iron-oxide deposits in the process of chemical decontamination of SIER will primarily be determined by the complete dissolution of hematite, which is formed from magnetite and goethite at elevated temperatures, for example, in the cooling water of the reactor [16]. Hematite is difficult to dissolve in mineral acids compared to magnetite [17] and is practically not removed from SIER during ultrasound treatment. In the presence of chelating agents such as EDTA, IDA, and NTA, the hematite solubility is also lower than that of magnetite, which is associated with a more stable lattice [18,19]. An effective solution is the reductive dissolution of hematite using organic compounds – ascorbic or oxalic acid, as well as the addition of Cu(I) and Sn(II) salts [20]. The rate of hematite dissolution is affected by the particle size and the process temperature [21–23]. Reduced Fe^{2+} is added to the solution, which in turn contributes to the further dissolution of hematite due to the redistribution of the electron density between Fe^{2+} in the aqueous phase and Fe^{3+} in the crystalline phase of the oxide. The rate-limiting stage of this dissolution process will be the transition of Fe^{2+} to the aqueous phase [24]. However, the presence of dissolved oxygen in the system will lead to significant inhibition of dissolution due to Fe^{2+} oxidation [25].

The method of electrochemical regeneration of SIER is promising [26,27]. This method involves the treatment of SIER in citrate solutions and the addition of ascorbic acid, which will lead to a partial reduction of iron with the transition to the dissolved form in the form of complex compounds. As a result of the accompanying electrochemical treatment at the cathode, a gradual reduction of metallic iron occurs, which reduces the volume of secondary radioactive waste. However, the efficiency of SIER decontamination by this method does not exceed 40%; in addition, the works do not provide information about the dissolution efficiency of iron-oxide deposits.

Undoubtedly, the reduction dissolution of hematite is a fairly effective method for SIER cleaning from iron-oxide deposits; however, the introduction of organic compounds can create some difficulties in cleaning the resulting secondary radioactive waste. It is due to the formation of solid cobalt complexes such us $Co(Ox)_2^{2-}$, $Co(Ox)_3^{4-}$, $[CoH_2Asc]^{2+}$, $[Co_2(Cit)_2(H_2O)_4]^{2-}$, $[Co_2(Cit)_2]^{2-}$ etc. (where Ox – oxalates, Asc – ascorbates, Cit – citrates); therefore, the problem of subsequent extraction or concentration of radionuclide from secondary liquid radioactive waste cannot be solved using precipitation or sorption techniques.

Decontamination of SIER with mineral acid solutions without addition of organic compounds can be an effective way of processing. Intensification of the dissolution process of iron-oxide deposits can be carried out using direct current, by additional processing of SIER in the cathode space. This work is devoted to evaluating the effectiveness of model SIER decontamination with mineral acid solutions, including with the use of direct current.

2. Experimental

2.1. Material and reagents

Iron chloride (III) ($FeCl_3 \times 6H_2O$), iron sulfate (II) ($FeSO_4 \times 7H_2O$), ammonium hydroxide (NH_4OH), sodium hydroxide (NaOH), sodium nitrate ($NaNO_3$), a hydrochloric acid solution with a concentration of 11.3 mol/l (HCl), a sulfuric acid solution with a concentration of 17.5 mol/l (H_2SO_4), and a nitric acid solution with a concentration of 13.3 mol/l (HNO_3) of high-grade qualifications were purchased in LLC NevaReaktiv, Russia and used as such. The Co-57 radionuclide in 1 M HCl solution was purchased in the Leypunsky Institute of Physics and Power Engineering. The cation exchanger KU 2–8 was purchased in the «TOKEM » company, Russia. Before starting work, the cation exchanger was washed with 1 M of HNO_3 solution under dynamic conditions, after which it was washed from the acid residues with distilled water and stored in a glass stoppered bottle. Magnetite and hematite powders simulating crud removed from the reactor core were synthesized according to the scheme published in Ref. [28].

2.2. Synthesis and characteristics of model SIERs contaminated with iron-oxide deposits

SIERs were obtained using a modified technique described in Ref. [28], with the difference that the resins were not additionally washed after contact with iron salts solutions to form additional model deposits on the surface of ion-exchanger grains. Ion exchange resin KU 2–8 in H-form of a volume of 50 ml was placed in a column of an internal diameter of 40 mm, and distilled water labeled with Co-57 radionuclide was passed at a rate of 2 column volumes per hour.

To obtain a KU-Hem sample, the resin was transferred to a solution of $FeCl_3$ of a concentration of 0.5 mol/L (250 mL). The produced pulp was stirred for 24 h and, then, alkalized by a solution of NH_4OH of a concentration of 10 mol/L until neutral reaction and additionally held for 3–6 h. Thereafter, the pulp was acidified by a solution of HCl until pH 2 and immediately transferred to the autoclave with subsequent hydrothermal treatment at 175 °C for 24 h.

To obtain a KU-Mag sample, the resin was transferred to a solution of a volume of 250 mL containing $FeCl_3$ and $FeSO_4$ of concentrations of 0.15 and 0.45 mol/L, respectively. The produced pulp was stirred for 24 h and, then, alkalized by a solution of NH_4OH of a concentration of 10 mol/L until neutral reaction and additionally held for 3–6 h. Thereafter, the pulp was additionally alkalized by a solution of NH_4OH until pH 13–14 and immediately transferred to the autoclave with subsequent hydrothermal treatment at 175 °C for 24 h.

After processing, the SIER samples were washed by decantation from the iron oxide particle residues formed outside the ion-exchanger grains, after which they were treated under dynamic conditions with a solution of the following composition: HNO_3 – 3 mol/l, $NaNO_3$ – 1 mol/l with a volume of 500 ml. Prepared SIERs contaminated with iron-oxide deposits were stored in a wet state in a glass-stoppered bottle. To evaluate the dissolution efficiency and rate on iron-oxide deposits, similar SIER models were prepared but without Co-57.

Fig. 1 shows images of resins obtained using an optical microscope and scanning electron microscopy. The KU-Mag sample is optically opaque (Fig. 1a), and the grain surface is covered with an even layer of magnetite that prevents the light beam from passing (Fig. 1b). The bulk of iron is located in the upper layer with a thickness of 35 μm, which contrasts with the rest of the volume (Fig. 1c). The KU-Hem sample is partially transparent and has a red color in an intense light beam due to the presence of evenly distributed hematite in the ion-exchanger grain matrix (Fig. 1a*). The surface of KU-Hem is covered with hematite flakes that peel off when exposed to mechanical action (Fig. 1b*). In the grain matrix, iron is distributed relatively evenly with a layer of increased content 10 μm thick.

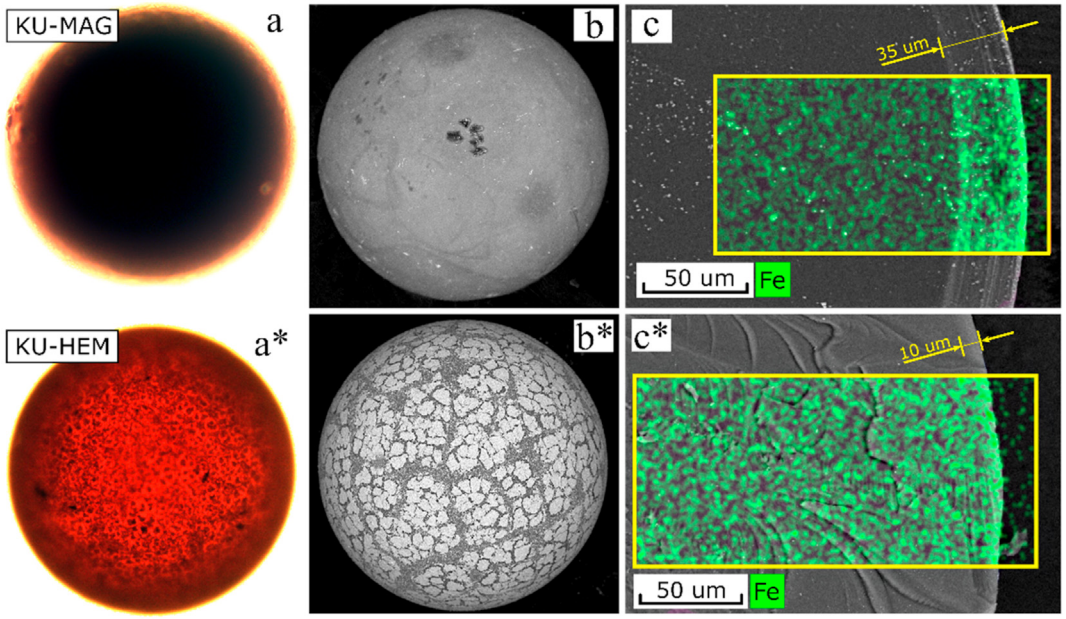

Fig. 1. Model ion-exchangers obtained during the work; a, a* – images of ion-exchangers obtained in an optical microscope, b, b* – SEM images of ion-exchangers, c, c* – distribution of iron on the surface of the resin grain section.

2.3. Dissolution of Oxide Powders and Deposits on model SIERs with Mineral Acid Solutions

The dissolution of iron oxide powders depending on the concentration of the acid solution was evaluated under static conditions with continuous mixing for 7 days. The V/m ratio was 10 ml/g, the sample weight was 0.2 g. After that, the powders were separated by centrifugation and the iron content in the acid solution was determined using atomic absorption spectrometry.

The dissolution of iron-oxide deposits on model SIERs in concentrated solutions of HNO_3 and HCl was carried out under static conditions. To do this, an aliquot of an acid solution of a known volume was added to an air-dry sample of the model SIER weighing 0.5 g, followed by continuous mixing. After 7 days, the resin was separated by decantation from the solution, in which the concentration of iron was determined, after which a fresh portion of the acid solution was added and the operation was repeated.

The effect of Fe^{2+} on the complete deactivation of model SIERs was evaluated by determining the specific activity of the acid solution after 7 days, the ratio V/m – 250 ml/g, and the weight of the air-dry resin sample – 0.2 g.

The completeness of dissolution of iron-oxide deposits on SIER, as well as the completeness of decontamination, was calculated by equation (1):

$$DS = \left(\frac{A_s \times V_s}{A_r}\right) \times 100 \quad (1)$$

where A_s – the activity of the acid solution (Bq/ml) or iron concentration (mg/ml), V_s – the volume of acid solution (ml), A_r – the initial activity of the sample resin (Bq) or source specific iron content (mg). The relative error of determination of the iron concentration using the atomic absorption flame spectroscopy did not exceed 5%. The error of determination of the specific activity of Co-57 using the gamma-spectroscopy did not exceed 10%.

2.4. Direct current processing of model SIERs

Processing of model SIERs was performed using an electrochemical cell, the design of which is shown in Fig. 2.

A cylindrical container with a volume of 100 ml made of 1.5-mm-thick borosilicate glass was the electrochemical cell chamber. The chamber was covered with a Teflon lid with a hole for removing gaseous products formed during electrolysis. A basket was placed to hold the model SIER in the cathode space in the electrochemical cell chamber. The walls of the basket were made of acid-resistant polymer mesh, which ensures free circulation of the solution between the cathode space and the electrochemical cell chamber. The basket diameter was 1.2 cm, the working volume – 3.6 ml.

The electrochemical cell used a platinum cathode, purity 99.99%, made in the form of a 0.5-mm-thick spiral with a working area of

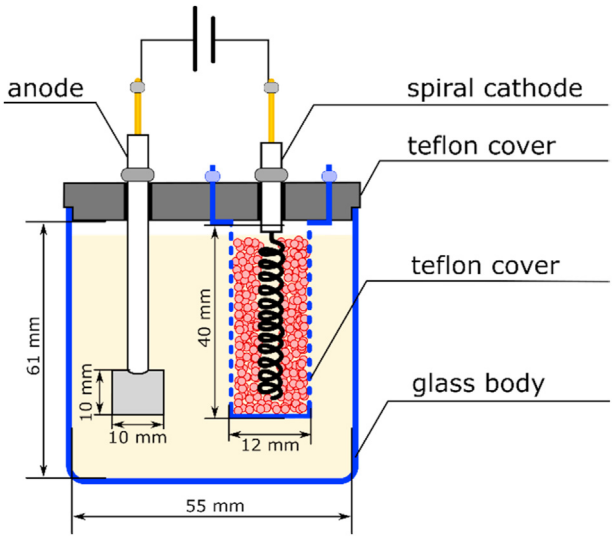

Fig. 2. Design of an electrochemical cell.

2.36 cm^2. A 0.2-mm-thick square plate of platinum with a purity of 99.99% and an area of 2 cm^2 was used as an anode. The process was performed using a direct current power source in the current stabilization mode.

To evaluate the dissolution efficiency and rate of SIERs iron-oxide deposits, a fixed volume of solution (1–2 ml) was sampled at certain time intervals during electrochemical treatment, in which the iron concentration was determined. The sampled part of the working solution was filled with a fresh acid solution, which was later taken into account in the calculations. Every 6–12 h, depending on the electrochemical treatment mode, the volume of the working solution was filled with a fresh portion of distilled water. For the effectiveness of SIER decontamination, a solution with a volume of 10 ml was sampled at certain time intervals and the specific activity was measured. After the measurement, the solution was returned to the electrochemical cell. The processing modes are shown in Table 1. The dissolution efficiency of iron-oxide deposits without electrochemical treatment was evaluated alongside, modes No. 1, 3, 6, 8, 11.

To control the residual iron content in model SIERs, the ion-exchangers were separated from the solution, washed on a filter with 250 ml of distilled water, and dried at 80 °C for 6 h. The dried ion-exchangers were crushed and filled with a fixed volume of HCl solution with a concentration of 10 mol/l and kept for a day under heating and periodic mixing. After that, the hydrochloric acid solution was diluted with distilled water of a fixed volume, and the iron concentration was determined.

2.5. Hardware and software

The iron content in the working solution was evaluated using atomic absorption flame spectroscopy using a Thermo Solar AA M6 instrument (Thermo Electron Corporation, USA). Co-57 specific activity (photopeak energy: 122 keV) was determined by the direct radiometric method using a gamma-radiometer RKG-AT1320 equipped with a NaI(Tl) detector measuring 63 × 63 mm (RPE Atomtech, Republic of Belarus). Surface structure images of the investigated materials were obtained by the means of scanning electron microscopy on a Carl Zeiss CrossBeam XB 1540 (Germany) microscope with an addon for energy dispersive analysis. X-ray phase analysis was performed on a D8 ADVANCE diffractometer; X-ray images of samples were recorded in the range of angles 2θ 3–85° with a step of 0.02° with a count at 0.6 s. The phase composition was identified using the Qualx2.0 program [29]. The results were processed using the SciDavis program (version 1.23).

Table 2
The dissolution efficiency of magnetite and hematite in acids solution of various concentrations.

Concentration (mol/l)	Dissolution efficiency (%)					
	Magnetite			Hematite		
	HCl	HNO_3	H_2SO_4	HCl	HNO_3	H_2SO_4
1	99.3	70.5	98.4	21.6	0	2.8
2.5	100	100	99.4	68.1	0	9.7
5	100	100	62.9	99.0	0	97.6
7.5	100	100	49.8	98.8	0	96.5
9.5	100	100	50.9	99.7	99.5	92.1

3. Results and discussion

3.1. Iron-oxide deposits dissolution under static conditions

Table 2 shows the results of the magnetite powder dissolution depending on the acid solution concentration. In HCl and HNO_3 solutions with a concentration of 2.5–9.5 mol/l, the magnetite powder was dissolved completely. It was also found that when using H_2SO_4 solutions, the dissolution efficiency was inversely proportional to the concentration.

When using a solution of H_2SO_4 with a concentration of more than 5 mol/l, the formation of a white precipitate was recorded, which was represented by the hohmannite phase $(Fe_2(H_2O)_4((-SO_4)_2O)(H_2O)_4$. Thus, the apparent decrease in the dissolution rate of iron oxides is associated with the formation of poorly soluble salts.

Hematite, in contrast to magnetite, shows relative resistance to dissolution in solutions of mineral acids, which is confirmed by the experimental results given in Table 2. For example, dissolution in HNO_3 occurs only when concentrated solutions are used. In H_2SO_4 solutions, the effect of hohmannite formation is shown to a lesser degree, and a satisfactory degree of hematite dissolution is achieved at a concentration of 5 mol/l.

Fig. 3 shows dissolution diagrams of iron-oxide deposits from model SIERs with HCl and HNO_3 solutions at a concentration of 9.5 mol/l. The H_2SO_4 solution was not used due to the formation of poorly soluble complex salts. The dissolution of iron-oxide deposits on model SIERs is much worse in comparison with pure powders. The use of HCl is quite effective; however, the volume of concentrated acid solution spent on dissolving 95% of iron-oxide deposits exceeds 20 ml, which may be economically impractical. The use of the HNO_3 solution to dissolve hematite deposits is inefficient.

Despite the high efficiency of dissolving iron-oxide deposits with HCl solutions, their use in real conditions is limited or

Table 1
Resin treatment modes and the dissolution efficiency of hematite deposits.

Processing mode (No.)	Acid		Processing conditions		Hematite dissolution efficiency (%)
	Type	Concentration (mol/l)	Current strength (A)	Voltage (V)	
1	HNO_3	1	–	–	1.6
2		1	1	5.6	44.7
3		3	–	–	16.9
4		3	0.5	2.8	53.9
5		3	2.0	Var[a]	53.6
6	H_2SO_4	0.1	–	–	1.7
7		0.1	0.5	9.9	48.7
8		1.0	–	–	57.7
9		1.0	0.5	3.0	82.2
10		1.0	1.0	3.7	99.3
11		2.0	–	–	98.4
12		2.0	2.0	5.0	99.7

[a] Var – changed during the experiment.

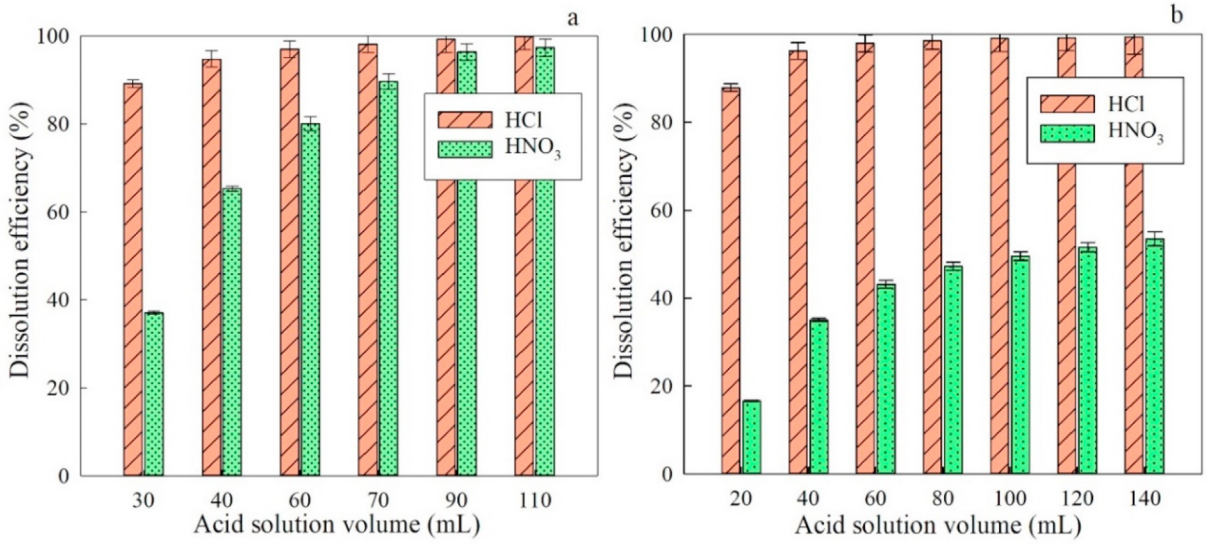

Fig. 3. Diagrams of dissolution of iron-oxide deposits with mineral acid solutions of concentrations 9.5 mol/l, a – KU-MAG, b – KU-HEM, the weight of the resin sample is 0.5 g.

completely prohibited due to rapid corrosion of steel structures in the presence of chloride ions [30], the removal of which from technological solutions in radiochemical production is a complex technological task [31,32]. For this reason, the results obtained using HCl solutions are considered for idealized objects of comparison, and further work on the electrochemical dissolution of iron-oxide deposits was carried out with HNO_3 and H_2SO_4 solutions.

Fig. 4 shows diagrams of the desorption efficiency of Co-57, used as an indicator of the efficiency of iron-oxide deposits dissolution, from a KU-HEM sample with solutions of H_2SO_4 and HNO_3 in the presence of $FeSO_4$, as well as $NaNO_3$ (3 mol/l), introduced to reduce the secondary adsorption of the radionuclide. It is known that Fe^{2+} can act as a reducing agent in reactions of the transformation of hardly soluble hematite into easily soluble magnetite; this process is called mushketovitization [33]. Such transformations occur as a result of the disproportionation reaction with the oxidation of Fe^{2+} in solution and the reduction of Fe^{3+} integrated into the hematite lattice, followed by its release into solution [34,35]. In neutral media, such processes occur through the formation of an amorphous $Fe(OH)_3$ or magnetite phase, which simplifies the dissolution process [36]. In this regard, it can be assumed that the addition of Fe^{2+} to the deactivating acid solution can increase the efficiency of hematite dissolution. However, adding Fe^{2+} leads to mixed results. When using HNO_3, the introduction of $FeSO_4$ leads to a slight increase in the desorption of Co-57 but the total efficiency of KU-HEM deactivation does not exceed 35%. The use of non-concentrated H_2SO_4 solutions allows increasing the completeness of hematite deposits dissolution; the decontamination efficiency when using 1 M solution reaches 80%. The introduction of Fe^{2+} does not have a noticeable effect on the dissolution efficiency, and at a concentration of more than 10^{-2} mol/l, on the contrary, it leads to a decrease.

3.2. Electrochemical dissolution of iron-oxide deposits

Since iron-oxide deposits in the form of hematite can be

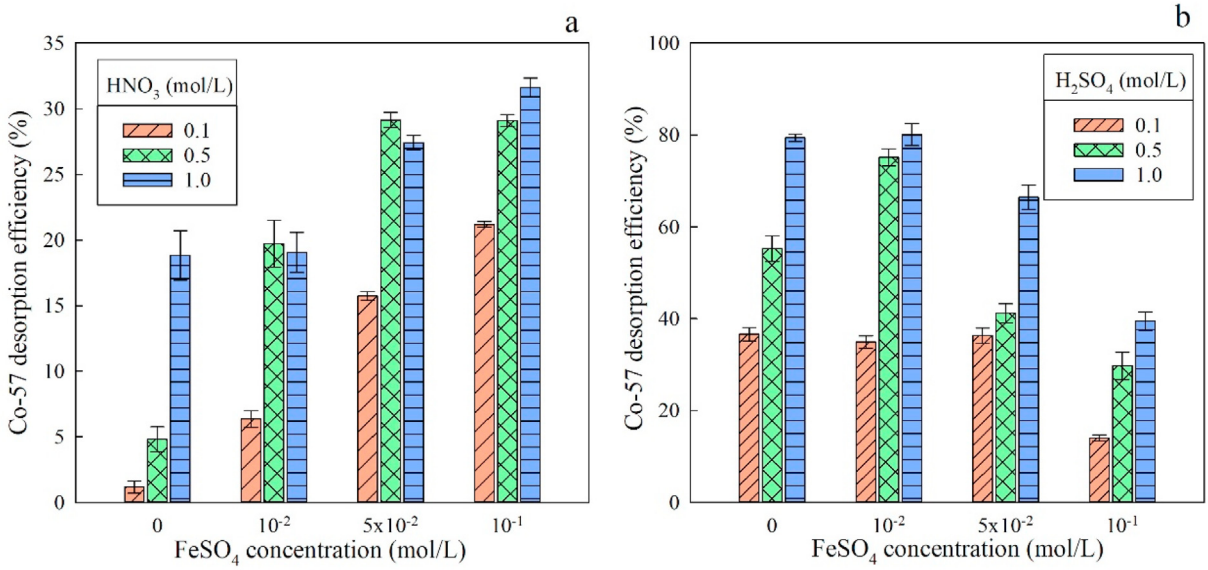

Fig. 4. Desorption of Co-57 from KU-HEM with a – HNO_3 solutions, b – H_2SO_4 solutions in the presence of Fe^{2+}, V/m ratio – 250 ml/g, m – 0.2 g.

relatively easily dissolved using solutions of available mineral acids, further work on electrochemical dissolution was carried out with the KU-Hem sample.

Additional treatment of SIER in the presence of direct current can increase the efficiency of hematite dissolution, which is associated with the following reactions:

- $2H^+ + 2\bar{e} \rightarrow 2H_2\uparrow$ (cathode)
- $2H_2O - 4\bar{e} \rightarrow O_2\uparrow + 4H^+$ (anode)
- $Fe_2O_3 + 6H^+ + 2\bar{e} \rightarrow 2Fe^{2+}_{(aq)} + 3H_2O$ [34].

Thus, in the cathode space, hematite dissolution is intensified due to the reduction processes. Fig. 5 shows the dissolution curves of iron-oxide deposits when using a nitric acid solution.

When using nitric acid, a noticeable effect on the hematite dissolution is detected at a concentration of 3 mol/l, while an increase in the current strength from 0.5 A to 2.0 A is accompanied by a gradual increase in voltage (Fig. 5, curve 4), resulting in significant heating of the solution with subsequent precipitation of iron hydroxide. The reason for precipitation is the solution pH shift to the slightly alkaline area to 8.53 ± 0.1. This change is associated with the reduction of nitric acid to ammonia [37], which was clearly felt at the time of opening the electrochemical cell. In addition, at the end of the experiment, the anode was covered with a layer of dark coating, which presumably led to an increase in resistance and, as a result, voltage. Fig. 6 shows an X-ray image showing that the coating formed during the electrochemical treatment of the resin is represented by weakly crystallized phases of $FePt_3$ and FePt compounds. Thus, an increase in the current strength in the presence of nitric acid leads to the introduction of iron into the anode material, which leads to undesirable consumption of platinum and the electrode resource exhaustion.

Fig. 7 shows curves for the degree of dissolution of iron-oxide deposits from the surface of the ion exchange resin. With an increase in the concentration of the sulfuric acid solution and the current strength, both the rate and the degree of dissolution naturally increase. For electrochemical treatment modes No. 10 and 12, the degree of dissolution exceeds 99%; therefore, the use of sulfuric acid is more preferable. When using sulfuric acid, the formation of a coating on the anode or voltage changes did not occur.

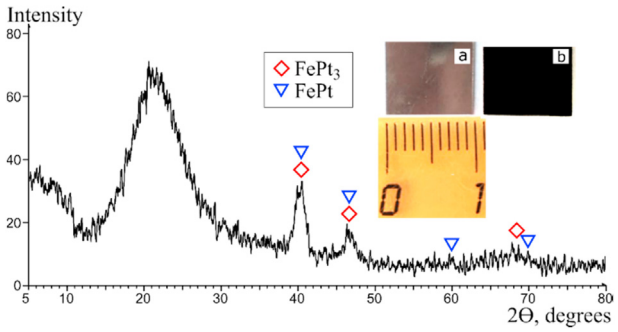

Fig. 6. X-ray image of the coating formed when using the treatment mode No. 5 (HNO_3 – 3 mol/l, 2A); figure on the inset a – the initial surface of the anode, b – the surface of the anode with a coating.

A comparison of the kinetic curves of chemical and electrochemical dissolution of hematite on model SIERs is shown in Fig. 8. In general, the rate and overall efficiency of electrochemical dissolution are higher than those of chemical treatment. However, the initial sections of the kinetic curves for chemical dissolution in the time interval of 10–600 min have a higher increase, which is probably due to slower mass transfer of dissolved iron from the basket to the sampling area.

Table 1 shows data on the residual iron content in model SIERs depending on the processing method. Treatment modes No. 1–9 are ineffective or ineffective for dissolving hematite. The use of electrochemical treatment makes it possible to increase the efficiency of hematite dissolution significantly in comparison with common washing with H_2SO_4 solutions. The completeness of dissolution is 99.3 and 99.7% for modes No. 10 and 12 respectively. It is worth noting that when ion-exchanger comes into contact with

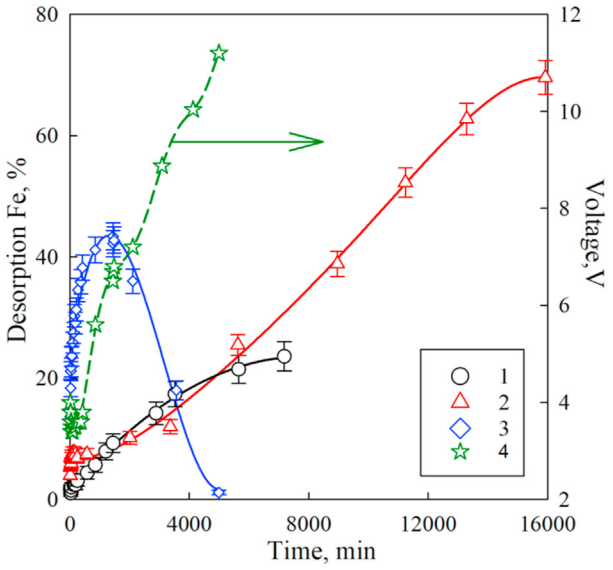

Fig. 5. Dependence of the dissolution degree of iron-oxide deposits from the surface of ion exchange resin contaminated with hematite on the time of electrochemical treatment; treatment mode 1 – No. 2 (HNO_3 – 1 mol/l, 1A, 5.6 V), 2 – No. 4 (HNO_3 – 3 mol/l, 0.5 A, 2.8 V), 3 – No. 5 (HNO_3 – 3 mol/l, 2A), 4 – the curve of voltage change during processing.

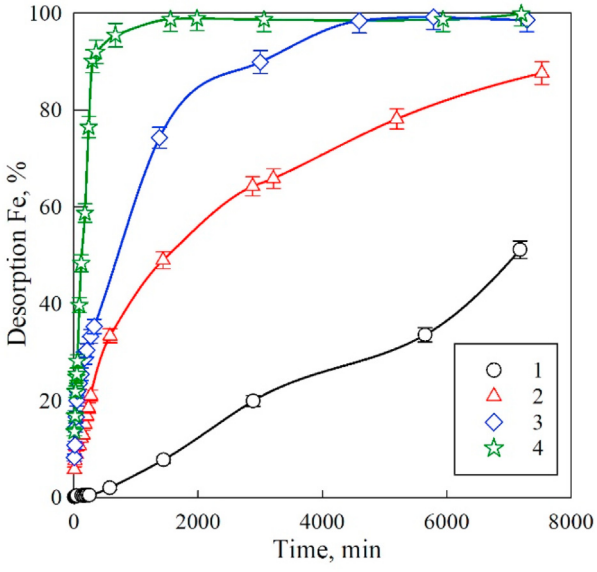

Fig. 7. Dependence of the dissolution degree of iron-oxide deposits from the surface of ion exchange resin contaminated with hematite on the time of electrochemical treatment; treatment mode 1 – No. 7 (H_2SO_4 – 0.1 mol/l, 0.5 A, 9.9 V), 2 – No. 9 (H_2SO_4 – 1 mol/l, 0.5 A, 3V), 3 – No. 10 (H_2SO_4 – 1 mol/l, 1A, 3.7 V), 4 – No. 12 (H_2SO_4 – 2 mol/l, 2A, 5V).

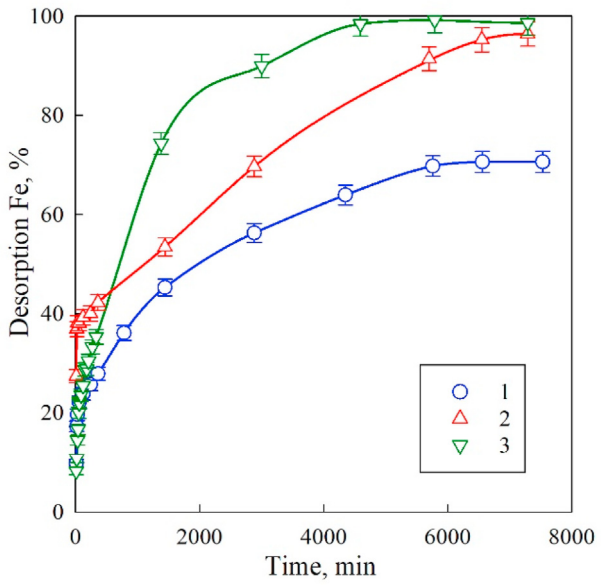

Fig. 8. Dissolution curves of hematite deposits on model SIERs, 1 – mode No. 8 (H_2SO_4 – 1 mol/l), 2 – mode No. 11 (H_2SO_4 – 2 mol/l), 3 – mode No. 10 (H_2SO_4 – 1 mol/l, 1A, 3.7 V).

2 mol/l of H_2SO_4 solution, the dissolution degree of hematite is 98.4%. However, the use of the electrochemical treatment mode No. 10 is more preferable, since when using a less concentrated H_2SO_4 solution, greater completeness of hematite deposits dissolution is achieved (99.3%), which reduces the cost of reagents and equipment corrosion.

3.3. Electrochemical decontamination

Fig. 9 shows the curve of KU-Hem decontamination depending on the time of electrochemical treatment. Since KU 2–8 is an ion-exchange resin which properties do not change during hydrothermal treatment [28], both the fixation of Co-57 radionuclide by iron-oxide deposits (fixed part) and its sorption during ion exchange on the functional groups of the resin (exchange part) occur. For this reason, the SIER decontamination curve passes through the maximum, which indicates the process of secondary adsorption of Co-57 radionuclide, which entered the H_2SO_4 solution due to the dissolution of hematite, at the ion-exchanger sorption centers. To remove the adsorbed radionuclide, the ion-exchangers, after electrochemical treatment, were additionally washed with a solution of the following composition: $NaNO_3$ – 2 mol/l, HNO_3 – 1 mol/l with a volume of 30 ml under dynamic conditions at a filtration rate of 5 bed volume per hour. As a result of this treatment, Co-57 photo peaks were not detected, which indicates complete deactivation of the model SIER.

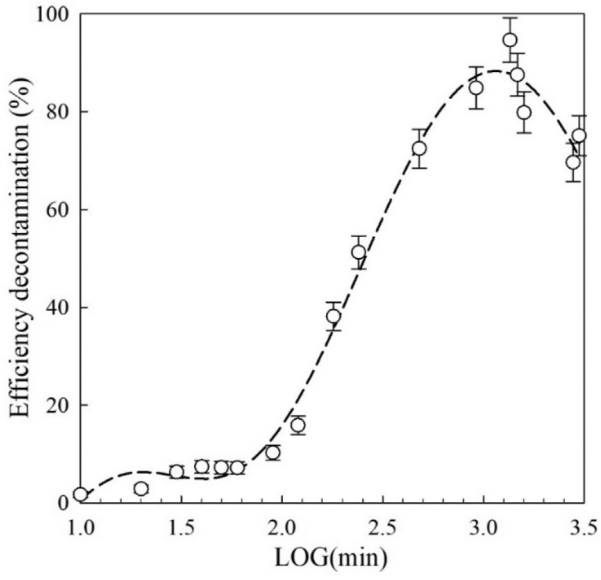

Fig. 9. Dependence of KU 2–8 GEM decontamination efficiency on electrochemical treatment time.

To reduce the volume of secondary waste, solutions after decontamination of model ion-exchangers were alkalized using NaOH. Changing the solution pH leads to precipitation of $Fe(OH)_3$ with simultaneous co-deposition of Co-57 radionuclide. After centrifugation, photo peaks of Co-57 were not detected in solutions, which indicates complete co-deposition of the radionuclide on the $Fe(OH)_3$ precipitate, the mass of which in the wet state was 0.2 g.

4. Conclusions

A method for electrochemical decontamination of SIER contaminated with iron-oxide deposits is proposed and tested by the example of model objects. As an electrolyte and deactivating solution, it is preferable to use H_2SO_4 solutions with a concentration of up to 1 mol/l. It is related to the fact that concentrated solutions lead to the formation of poorly soluble complex salts that reduce decontamination effectiveness, as well as due to equipment corrosion. The use of HNO_3 solutions is ineffective and can lead to anode contamination. With an increase in the concentration of the H_2SO_4 solution, as well as the direct current power, the rate and completeness of dissolution of hematite deposits and, respectively, the decontamination efficiency increase.

It is shown that this method allows for the fast and efficient dissolution of hematite particles in comparison with common acid treatment. The attractiveness of the method is that the additional reducing agents such as oxalic or ascorbic acids are not necessary. It is shown that the process of model SIERs deactivation is accompanied by the gradual dissolution of hematite followed by secondary adsorption of Co-57 on the functional groups of the ion-exchanger; therefore, additional treatment with sodium salts is required for the radionuclide desorption.

Funding

The authors gratefully acknowledge the Russian Science Foundation for supporting this work (Project 18-73-10066).

Declaration of competing interest

The authors declare that they have no known competing financial interests or personal relationships that could have appeared to influence the work reported in this paper.

Acknowledgments

Equipment of CUC “Far Eastern Center of Structural Investigations” was used in this work.

References

[1] J.A. Sawicki, Analyses of fuel crud and coolant-borne corrosion products in

normal water chemistry BWRs, J. Nucl. Mater. 419 (2011) 85–96, https://doi.org/10.1016/j.jnucmat.2011.08.032.
[2] J.A. Sawicki, P.J. Sefranek, S. Fisher, Depth distribution and chemical form of iron in low cross-linked crud-removing resin beds, Nucl. Instrum. Methods Phys. Res. Sect. B Beam Interact. Mater. Atoms 142 (1998) 122–132, https://doi.org/10.1016/S0168-583X(98)00231-6.
[3] M. Hoshi, E. Tachikawa, T. Suwa, C. Sagawa, C. Yonezawa, I. Aoyama, K. Yamamoto, Crud behaviors in high-temperature water, (I): characterization of water in JMTR OWL-1 loop, J. Nucl. Sci. Technol. 23 (1986) 511–521, https://doi.org/10.1080/18811248.1986.9735014.
[4] T.-L. Tsai, T.-Y. Lin, T.-Y. Su, H.-J. Wei, L.-C. Men, T.-J. Wen, Identification of chemical composition of CRUD depositing on fuel surface of a boiling water reactor (BWR-6) plant, Energy Procedia 14 (2012) 867–872, https://doi.org/10.1016/j.egypro.2011.12.1025.
[5] S. Chaturvedi, P.N. Dave, Removal of iron for safe drinking water, Desalination 303 (2012) 1–11, https://doi.org/10.1016/j.desal.2012.07.003.
[6] K. Otoha, T. Izumi, T. Hayashi, Y. Morikawa, H. Murabayashi, Crud removal performance with ion exchange resins in BWR plants, J. Nucl. Sci. Technol. 33 (1996) 10, https://doi.org/10.1080/18811248.1996.9731861.
[7] I. Inami, T. Baba, Study on the interaction between iron(III) hydroxide oxide and cation exchange resins, Bull. Chem. Soc. Jpn. 68 (1995) 2067–2072, https://doi.org/10.1246/bcsj.68.2067.
[8] S.D. Park, J.S. Kim, S.H. Han, K.Y. Jee, Distribution characteristics of ^{14}C and ^{3}H in spent resins from the Canada deuterium uranium-pressurized heavy water reactors (CANDU-PHWRs) of Korea, J. Radioanal. Nucl. Chem. 277 (2008) 503–511, https://doi.org/10.1007/s10967-007-7112-4.
[9] J. Li, J. Wang, Advances in cement solidification technology for waste radioactive ion exchange resins: a review, J. Hazard Mater. 135 (2006) 443–448, https://doi.org/10.1016/j.jhazmat.2005.11.053.
[10] K. Korpiola, J. Järvinen, K. Penttilä, P. Kotiluoto, Modeling of incineration of spent ion exchange resins of boiling water and pressurized water nuclear reactors, Nucl. Technol. 172 (2010) 230–236, https://doi.org/10.13182/NT10-A10908.
[11] V. Luca, H.L. Bianchi, F. Allevatto, J.O. Vaccaro, A. Alvarado, Low temperature pyrolysis of simulated spent anion exchange resins, J. Environ. Chem. Eng. 5 (2017) 4165–4172, https://doi.org/10.1016/j.jece.2017.07.064.
[12] L. Xu, X. Meng, M. Li, W. Li, Z. Sui, J. Wang, J. Yang, Dissolution and degradation of nuclear grade cationic exchange resin by Fenton oxidation combining experimental results and DFT calculations, Chem. Eng. J. 361 (2019) 1511–1523, https://doi.org/10.1016/j.cej.2018.09.169.
[13] T.-H. Cheng, C.-P. Huang, Y.-H. Huang, Y.-J. Shih, Kinetic study and optimization of electro-Fenton process for dissolution and mineralization of ion exchange resins, Chem. Eng. J. 308 (2017) 954–962, https://doi.org/10.1016/j.cej.2016.09.142.
[14] YuP. Korchagin, E.K. Aref'ev, E.Yu Korchagin, Improvement of technology for treatment of spent radioactive ion-exchange resins at nuclear power stations, Therm. Eng. 57 (2010) 593–597, https://doi.org/10.1134/S0040601510070104.
[15] M. Palamarchuk, A. Egorin, E. Tokar, M. Tutov, D. Marinin, V. Avramenko, Decontamination of spent ion-exchangers contaminated with cesium radionuclides using resorcinol-formaldehyde resins, J. Hazard Mater. 321 (2017) 326–334, https://doi.org/10.1016/j.jhazmat.2016.09.005.
[16] J. Zhao, J. Brugger, A. Pring, Mechanism and kinetics of hydrothermal replacement of magnetite by hematite, Geosci. Front. 10 (2019) 29–41, https://doi.org/10.1016/j.gsf.2018.05.015.
[17] P.S. Sidhu, Dissolution of iron oxides and oxyhydroxides in hydrochloric and perchloric acids, Clay Clay Miner. 29 (1981) 269–276, https://doi.org/10.1346/CCMN.1981.0290404.
[18] R. Torres, M.A. Blesa, E. Matijević, Interactions of metal hydrous oxides with chelating agents: IX. Reductive dissolution of hermatite and magnetite by aminocarboxylic acids, J. Colloid Interface Sci. 134 (1990) 475–485, https://doi.org/10.1016/0021-9797(90)90157-J.
[19] S.J. Keny, A.G. Kumbhar, G. Venkateswaran, K. Kishore, Radiation effects on the dissolution kinetics of magnetite and hematite in EDTA- and NTA-based dilute chemical decontamination formulations, Radiat. Phys. Chem. 72 (2005) 475–482, https://doi.org/10.1016/j.radphyschem.2003.12.055.
[20] Z.-Y. Lu, D.M. Muir, Dissolution of Metal Ferrites and Iron Oxides by HCI under Oxidising and Reducing Conditions, vol. 21, 1988, https://doi.org/10.1016/0304-386X(88)90013-8, 13 9-21.
[21] C.A. Lanzl, J. Baltrusaitis, D.M. Cwiertny, Dissolution of hematite nanoparticle aggregates: influence of primary particle size, dissolution mechanism, and solution pH, Langmuir 28 (2012) 15797–15808, https://doi.org/10.1021/la3022497.
[22] T. Echigo, D.M. Aruguete, M. Murayama, M.F. Hochella, Influence of size, morphology, surface structure, and aggregation state on reductive dissolution of hematite nanoparticles with ascorbic acid, Geochem. Cosmochim. Acta 90 (2012) 149–162, https://doi.org/10.1016/j.gca.2012.05.008.
[23] R. Salmimies, M. Mannila, J. Kallas, A. Häkkinen, Acidic dissolution of hematite: kinetic and thermodynamic investigations with oxalic acid, Int. J. Miner. Process. 110–111 (2012) 121–125, https://doi.org/10.1016/j.minpro.2012.04.001.
[24] Christophe Siffert, Barbara Sulzberger, Light-induced dissolution of hematite in the presence of oxalate. A case study, Langmuir 7 (1991) 1627–1634, https://doi.org/10.1021/la00056a014.
[25] M. Taxiarchou, D. Panias, I. Douni, I. Paspaliaris, A. Kontopoulos, Dissolution of hematite in acidic oxalate solutions, Hydrometallurgy 44 (1997) 287–299, https://doi.org/10.1016/S0304-386X(96)00075-8.
[26] L. Chi, J. Semmler, Electrochemical Regeneration of Spent Ion Exchange Resin (No. AECL-CW–127140-CONF-002), Atomic Energy of Canada Limited, 2010. http://inis.iaea.org/Search/search.aspx?orig_q=RN:49101522. (Accessed 4 November 2020).
[27] J. Semmler, L. Chi, Treatment of Liquid Waste and Regeneration of Spent Ion Exchange Resin Using Electrochemical Techniques (No. AECL-CW–127140-CONF-003), Atomic Energy of Canada Limited, 2012. http://inis.iaea.org/Search/search.aspx?orig_q=RN:49101523. (Accessed 4 November 2020).
[28] A. Egorin, E. Tokar, A. Kalashnikova, T. Sokolnitskaya, I. Tkachenko, A. Matskevich, E. Filatov, L. Zemskova, Synthesis and sorption properties towards Sr-90 of composite sorbents based on magnetite and hematite, Materials 13 (2020) 1189, https://doi.org/10.3390/ma13051189.
[29] A. Altomare, N. Corriero, C. Cuocci, A. Falcicchio, A. Moliterni, R. Rizzi, QUALX2.0: a qualitative phase analysis software using the freely available database POW_COD, J. Appl. Crystallogr. 48 (2015) 598–603, https://doi.org/10.1107/S1600576715002319.
[30] A.D. Mercer, E.A. Lumbard, Corrosion of mild steel in water, Br. Corrosion J. 30 (1995) 43–55, https://doi.org/10.1179/000705995798114177.
[31] M.L. Hyman, J.E. Savolainen, Removal of Chloride from Aqueous Solutions, US2919972A, 1960. https://patents.google.com/patent/US2919972A/en?oq=US+2919972+%D0%90. (Accessed 7 November 2020).
[32] I.A. Merkulov, D.V. Tikhomirov, A.I. Korobeinikov, A.S. Dyachenko, A. Yu Zhabin, G.A. Apalkov, V.A. Grigorieva, Method for Extracting Chloride-Ion from Nitrogen-Acute Technological Solutions of Radiochemical Manufacture, RU2678027C1, 2019. https://patents.google.com/patent/RU2678027C1/en?oq=RU+2678027. (Accessed 7 November 2020).
[33] A. Mücke, A. Raphael Cabral, Redox and nonredox reactions of magnetite and hematite in rocks, Geochemistry 65 (2005) 271–278, https://doi.org/10.1016/j.chemer.2005.01.002.
[34] S.V. Yanina, K.M. Rosso, Linked reactivity at mineral-water interfaces through bulk crystal conduction, Science 320 (2008) 218–222, https://doi.org/10.1126/science.1154833.
[35] K.M. Rosso, S.V. Yanina, C.A. Gorski, P. Larese-Casanova, M.M. Scherer, Connecting observations of hematite (α-Fe_2O_3) growth catalyzed by Fe(II), Environ. Sci. Technol. 44 (2010) 61–67, https://doi.org/10.1021/es901882a.
[36] B.-H. Jeon, B.A. Dempsey, W.D. Burgos, Kinetics and mechanisms for reactions of Fe(II) with iron(III) oxides, Environ. Sci. Technol. 37 (2003) 3309–3315, https://doi.org/10.1021/es025900p.
[37] G. Horanyi, F.M. Rizmayer, Catalytic activity of a tungsten carbide electrocatalyst in the reduction of HNO_3, HNO_2, and NH_2OH by molecular hydrogen, J. Electroanal. Chem. Interfacial Electrochem. 132 (1982) 119–128, https://doi.org/10.1016/0022-0728(82)85011-0.